Modelling of hybrid homopolar radial magnetic bearing considering flux leakage

Penghui Zhang*, Peng wen*, Yuexin Feng**, Jingchun Xu* and Zigang Deng*

* State Key Laboratory of Rail Transit Vehicle System, Southwest Jiaotong University, Chengdu 610031, China
** School of Information Science and Technology, Southwest Jiaotong University, Chengdu 611756, China
E-mail: deng@swjtu.cn

Abstract
Hybrid homopolar radial magnetic bearings (HHRMBs) combine the benefits of permanent magnet biasing and homopolar magnetic structures, offering high efficiency and low power consumption for high-speed and precision applications. However, the integration of permanent magnets introduces significant modeling challenges, particularly regarding flux leakage effects. This paper proposes a comprehensive modeling and design framework for HHRMBs, incorporating a refined equivalent magnetic circuit model calibrated by two-dimensional finite element method (2D FEM) analysis. The model explicitly accounts for flux leakage paths in both bias and control flux circuits, significantly improving prediction accuracy. A parametric design methodology is developed based on geometric relationships, enabling preliminary structural determination. Furthermore, a multi-objective optimization using the NSGA-II algorithm is implemented to balance electromagnetic force output, copper loss, and stator volume. Key design variables are selected via Latin hypercube sampling, and a feasible Pareto front is generated under practical constraints. The optimized configuration is validated through FEM simulations, demonstrating enhanced performance and model fidelity. The proposed framework offers a practical and extensible toolset for the design and optimization of advanced magnetic bearing systems.
Keywords : Hybrid homopolar magnetic bearing, flux leakage modeling, electromagnetic simulations

1. Introduction (括号方括号)

Active magnetic bearings (AMBs) were developed to address the inherent limitations of conventional mechanical bearings. They offer distinct advantages, including operation without lubrication concerns and the ability to achieve higher rotational speeds (Srinivas, 2018). By utilizing passive or actively controlled electromagnetic forces, AMBs enable non-contact rotor suspension, resulting in frictionless operation, reduced maintenance, low vibration, enhanced reliability, and superior rotational speeds. A key feature of AMBs is their tunable damping and stiffness characteristics, which can be adjusted during operation to meet diverse application requirements (Maslen, 2009. Malsen, 1996). These benefits have led to the widespread adoption of AMBs in applications such as industrial turbines, compressors, aerospace systems, energy storage, high-speed spindles, and medical devices (Huang, 2019, Huang 2023, Breńkacz, 2021, Kimman, 2010).

Radial magnetic bearings (RMBs) are generally categorized as homopolar or heteropolar based on their magnetic pole configurations. In homopolar designs, all poles share the same polarity within the radial plane, whereas heteropolar RMBs alternate polarity across orthogonal axes. Due to their structural simplicity and lower cost, heteropolar RMBs are more prevalent in industrial applications (Betancor,2 019). However, their higher power consumption and associated losses limit their efficiency and broader adoption. In contrast, homopolar RMBs inherently reduce power losses owing to their uniform polarity layout. To further improve efficiency, permanent magnets (PMs) can be introduced to replace the bias current, significantly lowering continuous power demand. This configuration, known as the hybrid homopolar radial magnetic bearing (HHRMB), combines the advantages of homopolar structure and biasing PM.

In general, the HHRMB offers several distinct advantages over heteropolar RMBs (Maslen, 2009, Huang, 2023, Lee, 1994, Lee, 1994, Kasarda, 1998, Li, 2023):

(1). Significantly reduced power consumption for equivalent load capacity or stiffness. In the absence of disturbance forces, the system operates with near-zero control power.

(2). Lower iron losses, including eddy current and hysteresis losses, due to the consistent polarity configuration. This characteristic makes HHRMB particularly suitable for applications such as flywheel energy storage systems, where heat dissipation is restricted in vacuum environments.

(3). Reduced copper losses, attributed to the elimination of bias currents through the integration of permanent magnets.

(4). Minimal cross-axis coupling and improved linearity between control current and electromagnetic force simplify the controller design and enhance system stability.

(5). Reduced hardware requirements, as only two sets of power amplifiers are needed to independently control the two orthogonal axes (x-axis and y-axis).

Despite its advantages, the HHRMB also presents several limitations:

(1). Increased axial length, inherent to its structure with PM, aggravates flux leakage and lowers the rotor's critical speed, thus limiting its maximum rotational capability.

(2). Higher design and manufacturing complexity, as the integration of PM complicates cost estimation, structural planning, and production processes.

(3). Reduced linearized displacement stiffness compared to bias-current-based configurations, which may impact system dynamic performance under high-precision requirements.

Owing to the aforementioned advantages, HHRMBs have attracted extensive research interest in modeling, structural design, and performance optimization. In the modelling of HHRMB, Meeker et al established an augmented circuit model for magnetic bearings by considering eddy current, fringing and leakage (Meeker, 1996). Sun investigated an asymmetric axial HMB for inertial platforms using a reluctance network model, validated by experimental results (Sun, 2016). Wang et al. proposed a conformal transformation-based analytical method to optimize axial load capacity and passive stiffness, which was experimentally confirmed via flywheel tests (Wang, 2013). To enhance model fidelity, some studies have introduced frequency-dependent reluctance in equivalent magnetic circuits (Zhu, 2005), while others explored novel hybrid topologies suitable for various magnetic levitation applications (Feng, 2010, Li 2008, Xu, 2014). Fang et al. designed an axial hybrid AMB with a secondary air gap to decouple control and bias flux paths, modeling the system via magnetic circuit theory and validating it experimentally (Feng, 2009). A combined radial-axial hybrid AMB incorporating permanent magnets was analyzed using extended circuit theory (Huang, 2007), and Yu proposed a hybrid modeling method combining subdomain and magnetic circuit approaches, demonstrating high accuracy against measurements (Yu, 2022). A design framework addressing eddy current losses for high-speed motors was proposed and verified experimentally in (Le, 2016). Han et al. extended the optimization of HHRMBs by incorporating dynamic performance analyses (Han, 2023).

Despite notable progress in the research on hybrid homopolar radial magnetic bearings, several critical limitations remain. First, the effect of flux leakage, particularly prominent with PM in HHRMB structure, has often been neglected or oversimplified in equivalent circuit models, resulting in reduced accuracy in electromagnetic analysis and design. To address the gaps, this paper presents a unified and practical framework for the modeling of HHRMBs with an improved equivalent magnetic circuit model incorporating flux leakage effects, calibrated and validated against FEM simulations.

2. Configuration of HHRMB

As shown in Fig. 1(a), the HHRMB consists of eight axially magnetized permanent magnet (PM) sectors, eight radial control coils, two laminated stators, two rotor rings, and two stator conductor rings. The PM sectors generate the bias magnetic flux, while the stators and rotor rings, made of laminated silicon steel, suppress eddy current losses. The solid stator yokes form the depart and return path for the bias flux. Fig. 1(b) illustrates the magnetic flux distribution: the bias flux flows axially through the PMs, stators, and rotor rings, forming four closed loops per stator plane; the control flux is confined within the radial plane of the stators. The add or subtract of bias and control fluxes determines the air-gap flux density.

The winding configuration is illustrated in Fig. 1(c). Coils located on opposite sides of a radial cross-section are connected in series, and further series-connected with coils on the corresponding side of the opposing stator. This arrangement allows full control of the two orthogonal axes using only two power amplifier sets, effectively minimizing the hardware complexity. A notable distinction from heteropolar designs is that only N-type or S-type poles appear along the circumferential direction in the radial stator plane.

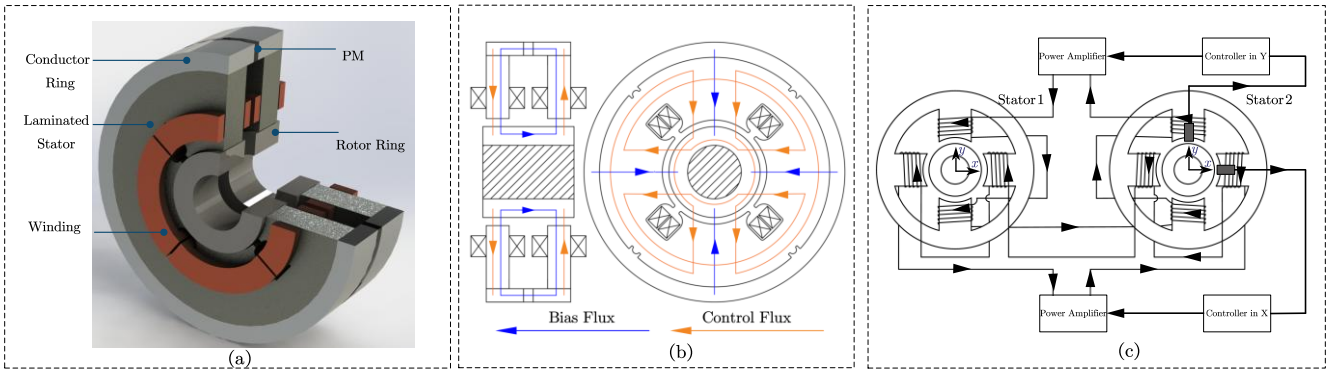

Fig. 1. HHRMB configuration (a), magnetic flux path diagram (b), and coil connection schematic (c).

3. Modelling of HHRMB

Accurate mathematical modeling of the HHRMB is crucial for its design, optimization, and controller design. This section employs the equivalent magnetic circuit method to analyze the bias and control flux paths separately. Initially, simplified models are established, and corresponding linearized electromagnetic forces are derived. Subsequently, the bias flux model is enhanced by incorporating flux leakage effects based on 2D FEM analysis to improve prediction accuracy. Finally, the accuracy of the proposed models is evaluated through comparison with FEM simulation results.

3.1 Simplified model of HHRMB

The simplified equivalent magnetic circuits for the bias and control flux are illustrated in Fig. 2(a) and Fig. 2(b), respectively. In these models, magnetic saturation, flux leakage, and the reluctance of stator conductors are neglected. The symbol Fpm and Rpm denote the magnetic motive force and magnetic reluctance of PM, respectively, while Φpm represents the total magnetic flux in the PM circuit. The air gap fluxes generated by the PM and control windings across the eight poles are denoted as Φp and Φc respectively, and NI refers to the magnetic motive force produced by control windings.

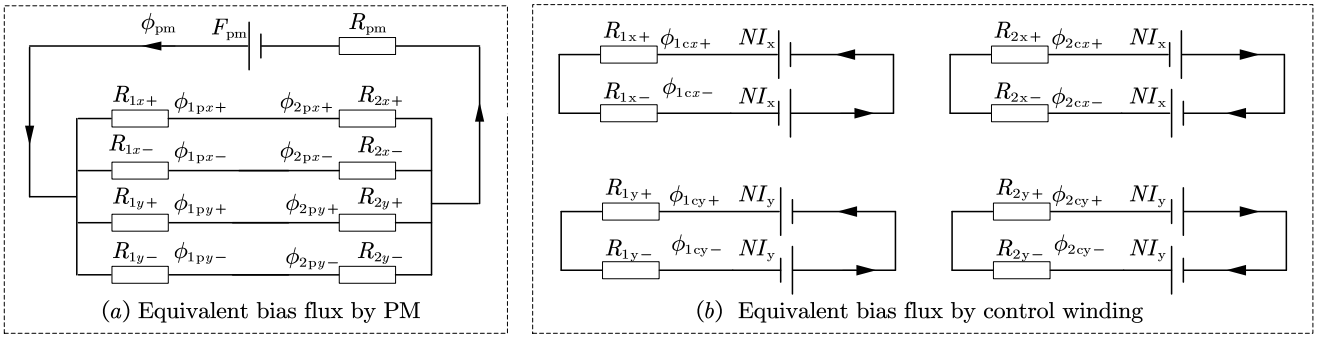

Fig. 2. Simplified equivalent magnetic circuits of PM bias flux (a) and control flux (b).

When the rotor is in the ideal centered position and the structure is assumed to be symmetric, the eight air-gap reluctances R1x+, R1x-, R1y+, R1y-, R2x+, R2x-, R2y+, R2y- are equal. This relationship can be expressed as:

$$\begin{bmatrix} R_{x+} & 0 & 0 & 0 & R_{pm} \\ 0 & R_{x-} & 0 & 0 & R_{pm} \\ 0 & 0 & R_{y+} & 0 & R_{pm} \\ 0 & 0 & 0 & R_{y-} & R_{pm} \\ 1 & 1 & 1 & 1 & -1 \end{bmatrix} \begin{bmatrix} \phi_{1px+} \\ \phi_{1px-} \\ \phi_{1py+} \\ \phi_{1py-} \\ \phi_{m} \end{bmatrix} = \begin{bmatrix} F_m \\ F_m \\ F_m \\ F_m \\ 0 \end{bmatrix} \tag{1}$$

Where, $R_{x+} = \dfrac{2(\delta_0 - \Delta\delta)}{\mu_0 A}$, $R_{x-} = \dfrac{2(\delta_0 + \Delta\delta)}{\mu_0 A}$, $R_{y+} = \dfrac{2(\delta_0 - \Delta\delta)}{\mu_0 A}$, $R_{y-} = \dfrac{2(\delta_0 + \Delta\delta)}{\mu_0 A}$. μ_0 and A denote the magnetic permeability of air and pole area, respectively.

The air gap magnetic flux density generated by the PM in one stator can then be expressed as:

$$\begin{bmatrix} \phi_{1\mathrm{px}+} \\ \phi_{1\mathrm{px}-} \\ \phi_{1\mathrm{py}+} \\ \phi_{1\mathrm{py}-} \end{bmatrix} = \begin{bmatrix} \dfrac{F_{\mathrm{m}} R_{\mathrm{i}}}{(R_{\mathrm{pm}} + R_{\mathrm{i}}) R_{\mathrm{x}+}} \\ \dfrac{F_{\mathrm{m}} R_{\mathrm{i}}}{(R_{\mathrm{pm}} + R_{\mathrm{i}}) R_{\mathrm{x}-}} \\ \dfrac{F_{\mathrm{m}} R_{\mathrm{i}}}{(R_{\mathrm{pm}} + R_{\mathrm{i}}) R_{\mathrm{y}+}} \\ \dfrac{F_{\mathrm{m}} R_{\mathrm{i}}}{(R_{\mathrm{pm}} + R_{\mathrm{i}}) R_{\mathrm{y}-}} \end{bmatrix} \tag{2}$$

Where, $R_i = R_{\mathrm{x}+} // R_{\mathrm{x}-} // R_{\mathrm{y}+} // R_{\mathrm{y}-} = \dfrac{R_{\mathrm{x}+} R_{\mathrm{x}-} R_{\mathrm{y}+} R_{\mathrm{y}-}}{(R_{\mathrm{x}-} R_{\mathrm{y}+} R_{\mathrm{y}-} + R_{\mathrm{x}+} R_{\mathrm{y}+} R_{\mathrm{y}-} + R_{\mathrm{x}+} R_{\mathrm{x}-} R_{\mathrm{y}-} + R_{\mathrm{x}+} R_{\mathrm{x}-} R_{\mathrm{y}+})}$.

Similarly, the four distinct magnetic flux densities on the same side of the stator, generated by the control windings, are related as follows:

$$\begin{cases} \phi_{1\mathrm{cy}+} = \phi_{1\mathrm{cy}-} = \dfrac{2NI_y}{R_y} \\ \phi_{1\mathrm{c}x+} = \phi_{1\mathrm{c}x-} = \dfrac{2NI_x}{R_x} \end{cases} \tag{3}$$

Due to the structural symmetry, only the y-axis is considered in the following magnetic force calculation. The total air-gap magnetic flux densities along the y-axis are:

$$\begin{cases} \phi_{1\mathrm{y}+} = \phi_{1\mathrm{py}+} + \phi_{1\mathrm{cy}+} \\ \phi_{1\mathrm{y}-} = \phi_{1\mathrm{py}-} + \phi_{1\mathrm{cy}-} \end{cases} \tag{4}$$

The total magnetic force generated along the y-axis of the entire HHRMB (comprising both stator parts) is expressed as:

$$F_{\mathrm{y}} = \frac{{\phi_{1\mathrm{y}+}}^2 - {\phi_{1\mathrm{y}-}}^2}{\mu_0 A} = \frac{(\phi_{1\mathrm{py}+} + \phi_{1\mathrm{cy}+})^2 - (\phi_{1\mathrm{py}-} - \phi_{1\mathrm{cy}-})^2}{\mu_0 A} \tag{5}$$

By applying a Taylor series expansion to Equation 5 at the balancing point $(\Delta\delta = 0,\ I_y = 0)$ and neglecting higher-order terms, the linearized magnetic force model is derived as:

$$F_{\mathrm{y}}(\Delta I_{\mathrm{y}}, \Delta\delta) = \left.\frac{\partial F_{\mathrm{y}}}{\partial \Delta\delta}\right|_{\substack{\Delta\delta=0 \\ \Delta I_y=0}} \Delta\delta + \left.\frac{\partial F_{\mathrm{y}}}{\partial \Delta I_{\mathrm{y}}}\right|_{\substack{\Delta\delta=0 \\ \Delta I_y=0}} I_{\mathrm{y}} = k_{\mathrm{I}} I_{\mathrm{y}} + k_{\delta} \Delta\delta \tag{6}$$

Where $k_I = \dfrac{F_{\mathrm{m}} N}{2\delta_0 \left(R_{\mathrm{pm}} + \frac{\delta_0}{2A\mu_0}\right)}$ and $k_{\delta} = -\dfrac{F_{\mathrm{m}}^2}{4A\mu_0\delta_0 \left(R_{\mathrm{pm}} + \frac{\delta_0}{2A\mu_0}\right)^2}$ are current stiffness and displacement stiffness, respectively.

Similarly, the magnetic force along the x-axis can be obtained by substituting the corresponding parameters. While the simplified model is straightforward, neglecting magnetic flux leakage may introduce significant calculation errors, particularly for the HHRMB structure that uses PMs for bias flux.

3.2 Improved model of HHRMB

To evaluate magnetic flux leakage in both the permanent magnet (PM) bias and control flux paths, 2-D finite element method (FEM) simulations are conducted for axial PM flux and radial control flux distributions, respectively. As is shown in Fig. 3, the PM-generated flux forms a closed loop in the axial direction, starting and ending in the PM after passing through the stator conductor rings, laminated stator poles, and rotor. The simulation reveals six primary leakage paths, denoted LF_{pm1}~ LF_{pm6}, with corresponding reluctances R_{lpm1}~ R_{lpm6}. To improve the accuracy of air-gap flux

density estimation, a refined magnetic circuit model incorporating PM flux leakage is established, as illustrated in Fig. 3.

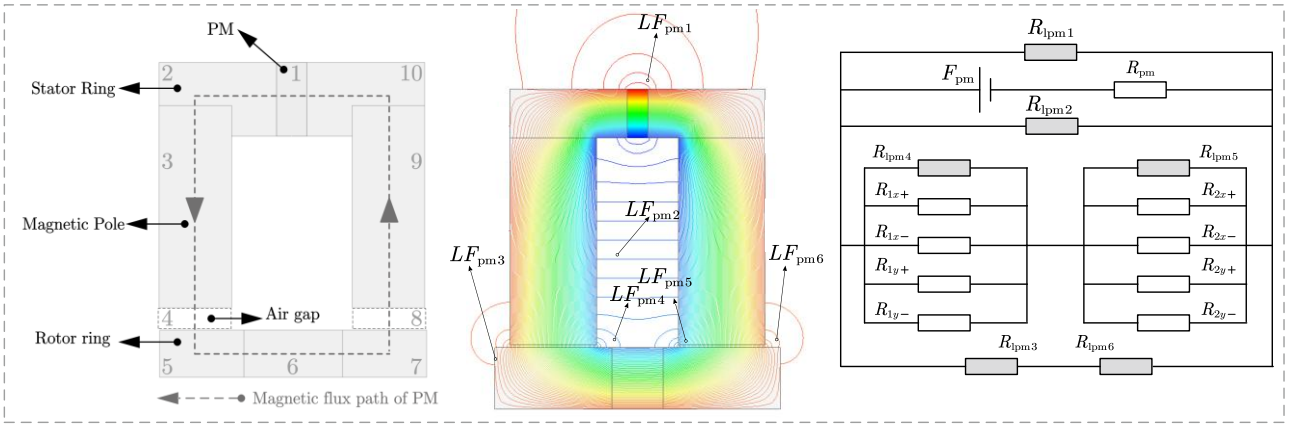

Fig. 3. Axial magnetic flux path and improved equivalent magnetic circuit model of PM.

The magnetomotive force (F_{pm}) and its reluctance (R_{pm}) of PM are expressed as:

$$\begin{aligned} F_{\mathrm{pm}} &= H_c l_{pm} \\ R_{\mathrm{pm}} &= \frac{l_{pm}}{\mu_r \mu_0 A_{\mathrm{pm}}} \end{aligned} \tag{7}$$

Where, H_{c}, l_{pm}, μ_{r} and A_{pm} are the coercive force, axial length, relative magnetic permeability and cross-sectional area of PM, respectively.

For notational simplicity, the following reluctance parameters ($\lambda_1 \sim \lambda_4$) are defined as：

$$\begin{aligned} \lambda_1 &= R_{\mathrm{lpm1}} // R_{\mathrm{lpm2}} \\ \lambda_2 &= \frac{R_1 R_{\mathrm{lpm4}}}{R_1 + R_{\mathrm{lpm4}}} \\ \lambda_3 &= \frac{R_2 R_{\mathrm{lpm5}}}{R_2 + R_{\mathrm{lpm5}}} \\ \lambda_4 &= R_{\mathrm{lpm3}} + R_{\mathrm{lpm6}} \end{aligned} \tag{8}$$

Where, $R_1 = R_{1\mathrm{y}+} // R_{1\mathrm{y}-} // R_{1\mathrm{y}+} // R_{1\mathrm{y}-}$ and $R_2 = R_{2\mathrm{y}+} // R_{2\mathrm{y}-} // R_{2\mathrm{y}+} // R_{2\mathrm{y}-}$.

The total equivalent reluctance of the magnetic circuit, excluding R_{pm}, can then be expressed as $R = \lambda_1 // (\lambda_2 + \lambda_3) // \lambda_4$. Consequently, the total magnetic flux (Φ_{pm}) in the circuit is given by:

$$\phi_{\mathrm{pm}} = \frac{F_{\mathrm{pm}}}{R_{\mathrm{pm}} + R} \tag{9}$$

The two air-gap magnetic fluxes in the y-axis direction generated by the PM in stator 1 can be expressed as:

$$\begin{cases} \phi_{1\mathrm{py}+} = \dfrac{\lambda_2 F_{\mathrm{m}}^*}{(\lambda_2 + \lambda_3) R_{1\mathrm{y}+}} \\ \phi_{1\mathrm{py}-} = \dfrac{\lambda_2 F_{\mathrm{m}}^*}{(\lambda_2 + \lambda_3) R_{1\mathrm{y}-}} \end{cases} \tag{10}$$

Where, $F_m^* = F_{\mathrm{pm}} - \phi_{\mathrm{pm}} R_{\mathrm{pm}}$.

The equivalent magnetic circuit for the control current along the y-axis of stator 1 is shown in Fig. 4. The control flux, excited by the control current, flows through the radial cross-section of the stator and rotor. The primary leakage paths, denoted $LF_{\mathrm{c1}} \sim LF_{\mathrm{c4}}$, correspond to leakage reluctances $R_{\mathrm{lc1}} \sim R_{\mathrm{lc4}}$. The reluctances $R_{\mathrm{s1}} \sim R_{\mathrm{s3}}$ represent the stator and rotor

reluctances along the main conduction path. The resulting two air-gap magnetic fluxes in the y-axis direction, Φ_{1cy+} and Φ_{1cy-}, can then be expressed as:

$$\begin{cases} \phi_{1cy+} = \dfrac{2NI_y R_{1c}}{R_{1y+}(R_{4c}+R_{3c}+R_{1c}+R_{2c}+2R_{s2})} \\ \phi_{1cy-} = \dfrac{2NI_y R_{2c}}{R_{1y-}(R_{4c}+R_{3c}+R_{1c}+R_{2c}+2R_{s2})} \end{cases} \tag{11}$$

Where, $R_{1c} = R_{lc1}//R_{1y+}//R_{lc2}$, $R_{2c} = R_{lc3}//R_{1y-}//R_{lc4}$, $R_{3c} = R_{s3}//R_{s3}$ and $R_{4c} = R_{s1}//R_{s1}$.

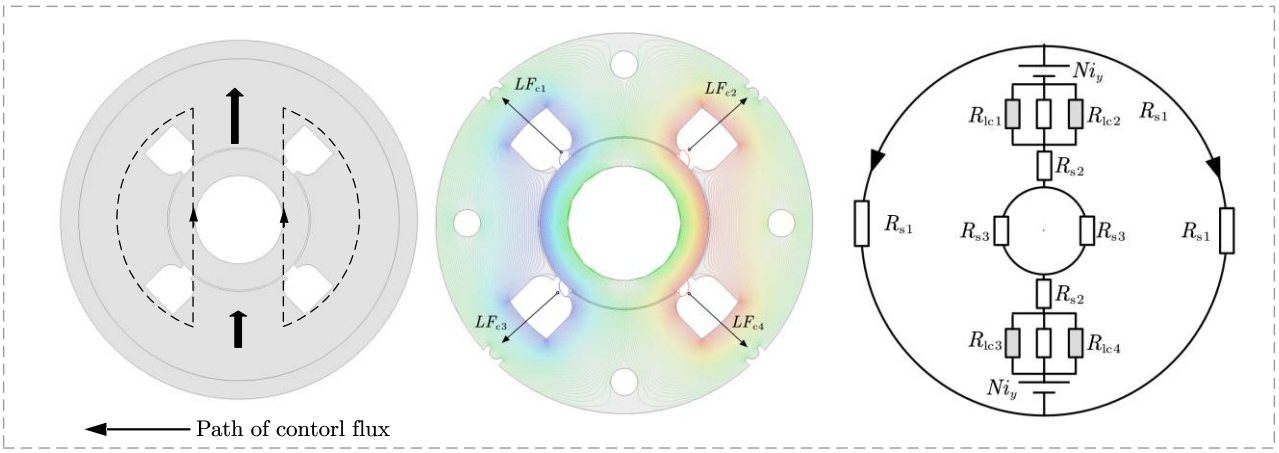

Fig. 4. Radial magnetic flux path and improved equivalent magnetic circuit model of control flux.

By substituting the calculated magnetic fluxes generated by the permanent magnet (Φ_{1py+}, Φ_{1py-}) and control winding (Φ_{1cy+}, Φ_{1cy+}) along the y-axis into Equation (5), the magnetic force in the y-axis under differential control mode can be obtained. To further validate the effectiveness of both the improved and simplified models, their respective results for magnetic flux density distribution along the air-gap circumferential direction are compared in Fig. 5, based on preliminary design parameters from Table. 2.

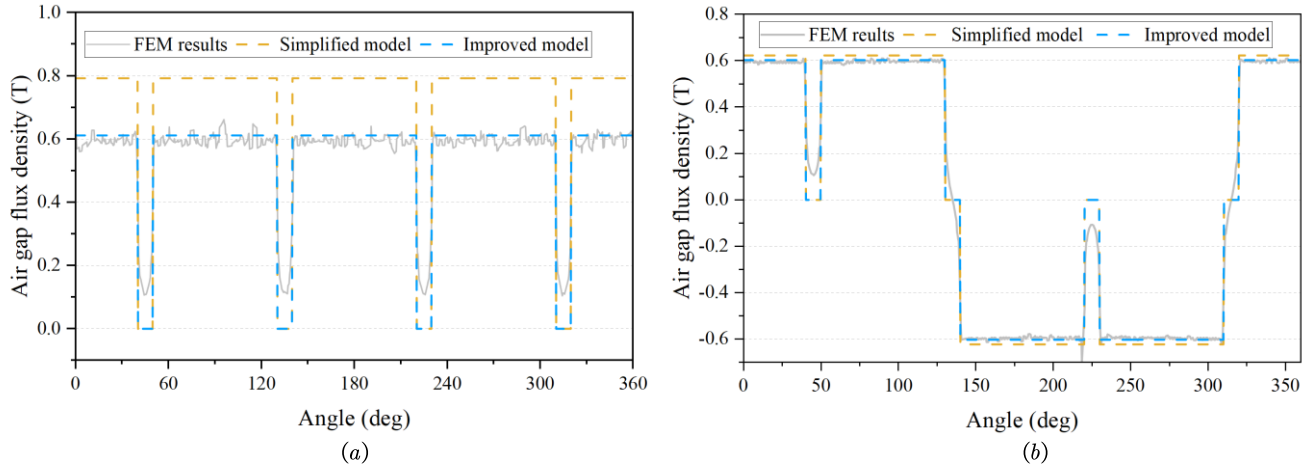

Fig. 5. Comparison of air gap magnetic flux density calculated by FEM, simplified model, and improved model: (a) PM-generated flux, (b) control winding generated flux..

Fig. 5(a) shows that the air-gap flux density induced by the PM in the improved model (0.61 T) closely matches the FEM result (average 0.60 T), significantly outperforming the simplified model (0.79 T). This improved accuracy results

from the consideration of flux leakage effects in the 2D simulation. In contrast, Fig. 5(b) indicates that the control winding flux results show only minor improvements compared to FEM (average 0.60 T), suggesting that the simplified model already provides sufficient accuracy for the control flux path, with limited benefit from incorporating leakage and conductor reluctance.

To further assess the improved model, Fig. 6 compares current stiffness and displacement stiffness among the FEM, simplified model, and improved model. As shown in Fig. 6(a), the displacement stiffness predicted by the improved model aligns well with FEM results and clearly surpasses the simplified model, primarily due to the consideration of PM flux leakage. Similarly, Fig 6(b) demonstrates that the improved model yields higher accuracy in current stiffness. However, the accuracy declines when the laminated silicon steel approaches magnetic saturation under higher control currents.

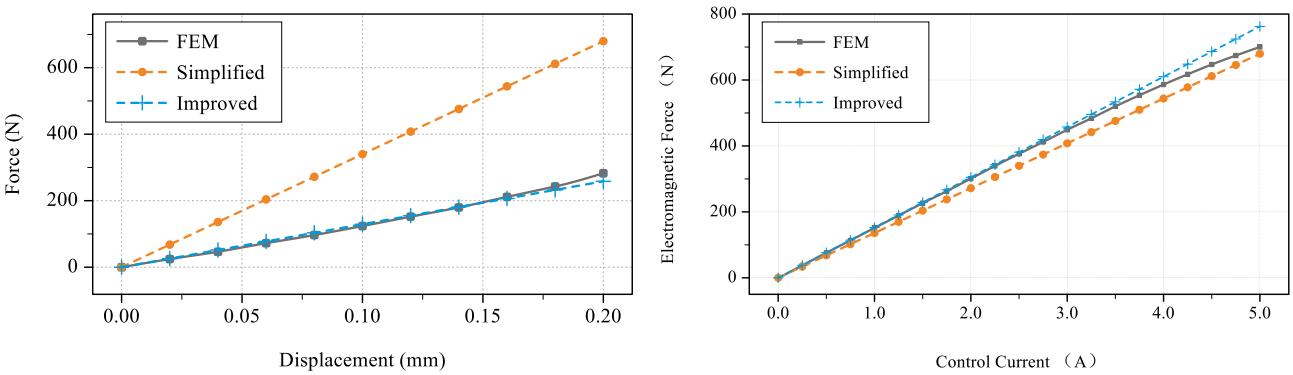

Fig. 6. Comparison of displacement stiffness (a) and control winding stiffness (b) for the simplified model, improved model, and FEM results.

4. Conclusions

In this paper, an enhanced equivalent magnetic circuit model incorporating flux leakage reluctance is proposed, based on insights obtained from detailed two-dimensional finite element method (2D FEM) simulations. The proposed model provides a more comprehensive representation of the magnetic behavior of the system, particularly for the permanent magnet (PM) branch. Validation results demonstrate that the improved PM circuit model exhibits excellent agreement with the FEM results across a range of operating conditions, confirming its effectiveness in capturing the essential magnetic phenomena.

The introduction of flux leakage reluctance into the PM path plays a crucial role in improving the model's accuracy, especially in regions with complex magnetic coupling and non-negligible stray flux. This modification significantly reduces discrepancies between analytical predictions and numerical simulations, enhancing the overall reliability of the equivalent circuit approach. However, the accuracy improvements observed in the modeling of the control winding circuit are relatively limited.

Overall, the enhanced model strikes a practical balance between computational efficiency and predictive accuracy, making it a useful tool for preliminary design and optimization of magnetic bearing systems.

References

[1] Srinivas, S. R., Tiwari, R. and Kannababu, C., Application of active magnetic bearings in flexible rotordynamic systems – a state-of-the-art review, Advances in Mechanical Engineering, Vol.106 (2018), pp.537–572.

[2] Maslen, E. H. and Schweitzer, G., Magnetic Bearings: Theory, Design, and Application to Rotating Machinery, Springer, Berlin, (2009).

[3] Maslen, E. H., Allaire, P. E., Noh, M. D. and Sortore, C. K., Magnetic bearing design for reduced power consumption, Journal of Tribology, Vol.118 (1996), pp.839–846.

[4] Huang, T., Zheng, M. and Zhang, G., A review of active magnetic bearing control technology, Proceedings of the 2019 Chinese Control and Decision Conference (CCDC), Nanchang, China, June 3–5, 2019, pp.2888–2893.

[5] Huang, Z., Li, C., Zhou, Z. et al., Magnetic bearing: structure, model, and control strategy, International Journal of

Advanced Manufacturing Technology, Vol.131 (2023), pp.3287–3333.
[6] Breńkacz, Ł., Witanowski, Ł., Drosińska-Komor, M. et al., Research and applications of active bearings: a state-of-the-art review, Mechanical Systems and Signal Processing, Vol.151 (2021), Article No.107423.
[7] Kimman, M. H., Langen, H. H. and Munnig Schmidt, R. H., A miniature milling spindle with active magnetic bearings, Mechatronics, Vol.20, No.2 (2010), pp.224–235.
[8] Betancor, J., Sahinkaya, M. N. and Zweiri, Y. H., Radial active magnetic bearing design optimization, Proceedings of the 10th International Conference on Rotor Dynamics – IFToMM, Rio de Janeiro, Brazil, September 23–27, 2019, pp.321–334.
[9] Lee, A. C., Hsiao, F. Z. and Ko, D., Analysis and Testing of Magnetic Bearing with Permanent Magnets for Bias, JSME International Journal, Series C: Dynamics, Control, Robotics, Design and Manufacturing, Vol.37, No.4 (1994), pp.774–778.
[10] Lee, A. C., Hsiao, F. Z. and Ko, D., Performance Limits of Permanent-Magnet-Biased Magnetic Bearings, JSME International Journal, Series C: Dynamics, Control, Robotics, Design and Manufacturing, Vol.37, No.4 (1994), pp.783–794.
[11] Kasarda, M. E. F., Allaire, P. E., Norris, P. M., Mastrangelo, C. and Maslen, E. H., Experimentally Determined Rotor Power Losses in Homopolar and Heteropolar Magnetic Bearings, Proceedings of the ASME 1998 International Gas Turbine and Aeroengine Congress and Exhibition, Vol.5, Stockholm, Sweden, June 2–5, 1998.
[12] Li, Q., Hu, Y. and Wu, H., Structure Design and Optimization of the Radial Magnetic Bearing, Actuators, Vol.12 (2023), Article No.27.
[13] Meeker, D. C., Maslen, E. H. and Noh, M. D., An augmented circuit model for magnetic bearings including eddy currents, fringing, and leakage, IEEE Transactions on Magnetics, Vol.32, No.4 (1996), pp.3219–3227.
[14] Sun, J., Wang, C. and Le, Y., Designing and Experimental Verification of the Axial Hybrid Magnetic Bearing to Stabilization of a Magnetically Suspended Inertially Stabilized Platform, IEEE/ASME Transactions on Mechatronics, Vol.21, No.6 (2016), pp.2881–2891.
[15] Wang, H., Liu, K. and Ao, P., Magnetic Field and Specific Axial Load Capacity of Hybrid Magnetic Bearing, IEEE Transactions on Magnetics, Vol.49, No.8 (2013), pp.4911–4917.
[16] Zhu, L. and Knospe, C. R., Modeling of Nonlaminated Electromagnetic Suspension Systems, IEEE/ASME Transactions on Mechatronics, Vol.15, No.1 (2010), pp.59–69.
[17] Seifert, R., Röbenack, K. and Hofmann, W., Rational Approximation of the Analytical Model of Nonlaminated Cylindrical Magnetic Actuators for Flux Estimation and Control, IEEE Transactions on Magnetics, Vol.55, No.12 (2019), Article No.8301016, pp.1–16.
[18] Zhu, L., Knospe, C. R. and Maslen, E. H., Analytic model for a nonlaminated cylindrical magnetic actuator including eddy currents, IEEE Transactions on Magnetics, Vol.41, No.4 (2005), pp.1248–1258.
[19] Jiancheng, F., Jinji, S., Hu, L. and Jiqiang, T., A Novel 3-DOF Axial Hybrid Magnetic Bearing, IEEE Transactions on Magnetics, Vol.46, No.12 (2010), pp.4034–4045.
[20] Li, Y., Li, W. and Lu, Y., Computer-Aided Simulation Analysis of a Novel Structure Hybrid Magnetic Bearing, IEEE Transactions on Magnetics, Vol.44, No.10 (2008), pp.2283–2287.
[21] Xu, S. and Fang, J., A Novel Conical Active Magnetic Bearing With Claw Structure, IEEE Transactions on Magnetics, Vol.50, No.5 (2014), Article No.8101108, pp.1–8.
[22] Jiancheng, F., Jinji, S., Yanliang, X. and Xi, W., A New Structure for Permanent-Magnet-Biased Axial Hybrid Magnetic Bearings, IEEE Transactions on Magnetics, Vol.45, No.12 (2009), pp.5319–5325.
[23] Huang, L., Zhao, G., Nian, H. and He, Y., Modeling and design of permanent magnet biased radial-axial magnetic bearing by extended circuit theory, Proceedings of the 2007 International Conference on Electrical Machines and Systems (ICEMS), Seoul, Korea (South), (2007), pp.1502–1507.
[24] Yu, C., Deng, Z., Chen, S., Mei, L., Peng, C. and Cao, X., A novel subdomain and magnetic circuit modeling method for hybrid homopolar radial magnetic bearings, Mechanical Systems and Signal Processing, Vol.170 (2022), Article No.108823.
[25] Le, Y. and Wang, K., Design and Optimization Method of Magnetic Bearing for High-Speed Motor Considering Eddy Current Effects, IEEE/ASME Transactions on Mechatronics, Vol.21, No.4 (2016), pp.2061–2072.
[26] Han, B., He, Z., Wen, T. and Zheng, S., Design, optimization and test of RHMB considering dynamic characteristics, International Journal of Mechanical Sciences, Vol.238 (2023), Article No.107847.